

Imaging Properties of the GBT Subreflector in C

Don Wells*

March 16, 1998

Abstract

The GBT Gregorian subreflector, an off-axis portion of an ellipsoid, images points in the neighborhood of its first focus onto points in the neighborhood of its second focus. Many of the pairs of points have identical separations, so that nearly-stigmatic imaging (nearly maximum gain) can be obtained for a variety of tilts and displacements of the subreflector. A grid of cases have been computed by ray tracing, and the results have been fitted with polynomials which are expressed in C. It is shown that, for imaging between points away from the foci, minimum phase error (maximum gain) will be obtained if the off-axis ellipsoid is tilted slightly; the optimum tilt is computed by a function expressed in C.¹

Contents

1	Introduction	2
2	Geometry of the GBT subreflector	2
3	Ray tracing analysis of the mapping from F_2 to F_1	3
4	Translation of bisector $(\Delta x_c, \Delta y_c)$ as a function of ΔS_{12} and $\Delta \phi$	6
5	Regression analysis: function <code>srEllipsoid()</code>	8
6	The ellipsoid phase error: function <code>srEllipsoidBestRms()</code>	11
A	The On-Axis Case – “For the Record”	12
B	Features expected to be added in future versions	14
	Bibliography	15

*mailto:dwells@nrao.edu

¹The two ellipsoid functions in C are included in ftp://fits.cv.nrao.edu/pub/gbt.dwells_src.tar.gz (237 KB).

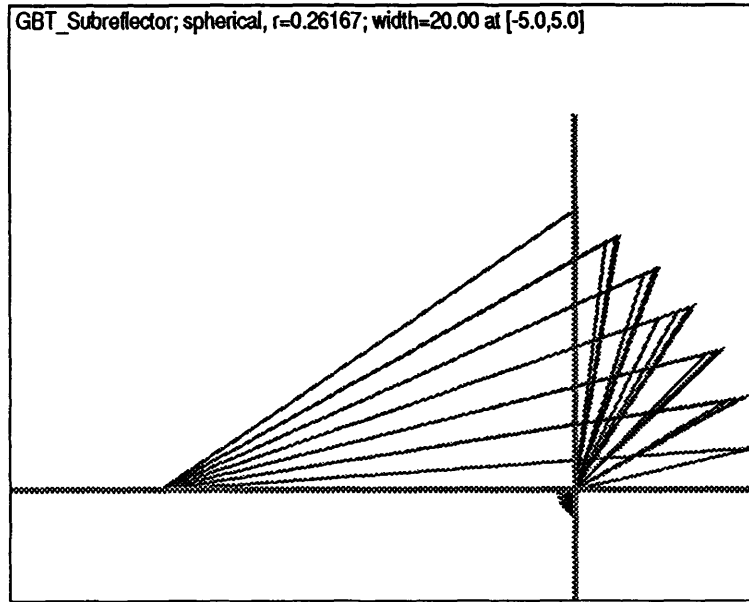


Figure 1: Overview of rays traced through the Subreflector

1 Introduction

The GBT feedarm, which carries both the Gregorian feeds and the Gregorian (ellipsoidal) off-axis secondary mirror (the subreflector), moves as a function of elevation with respect to the focal point of the GBT's 100 meter paraboloidal primary mirror. At the rigging angle elevation, the distance between the prime focal point and the Gregorian feedhorn is 11 meters, identical to the distance between the two foci of the subreflector, and the imaging can be accurately stigmatic if the subreflector is moved so that its two foci are coincident with the prime focal point and the feedhorn phase center. At other elevations the distance will not be 11 meters, and the ellipsoidal subreflector must operate away from its foci. The purpose of this GBT Memo is to present an analysis of how the subreflector forms nearly-stigmatic images in the neighborhoods of its two foci, including a discussion of how the nearly-spherical wavefront phase error varies with the orientation of the subreflector. The analysis is encapsulated in two C functions which are key elements of the GBT's Gregorian focus tracking algorithm [Wel98a].

2 Geometry of the GBT subreflector

The GBT Gregorian subreflector is an off-axis section cut from an ellipsoid by a conical surface: a cone originating at the second focal point of the ellipsoid and with opening half-angle $\theta_H = \pm 14.99^\circ$ [NS96, p.5] defines the edge of the subreflector. The overall geometry for a single cone of rays is shown in Figure 1 above. A spherical wave originating at the phase center of a Gregorian feedhorn, if it is coincident with the second focal point of the ellipsoid at the rigging angle, is imaged at the first focal point of the ellipsoid and will illuminate the off-axis paraboloidal main mirror. The next section will discuss what happens when the focal points and phase centers are not coincident.

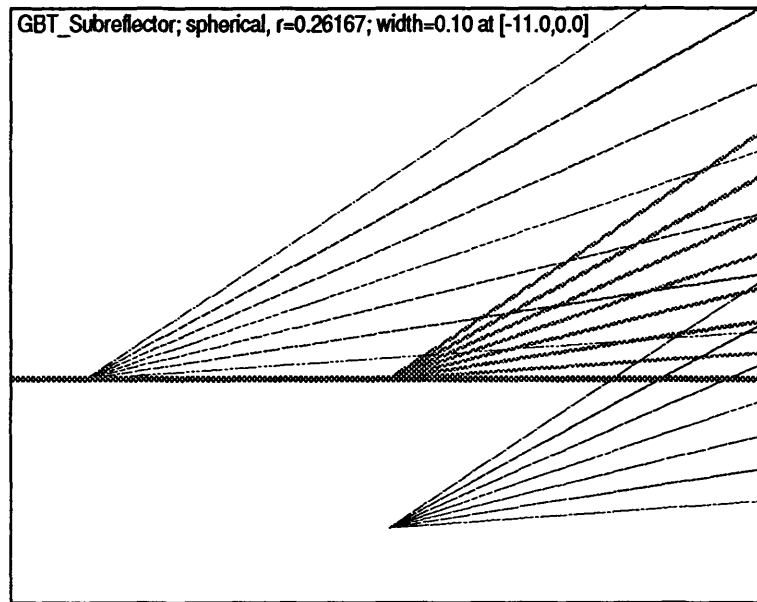


Figure 2: Three spherical waves emitted near the F_2 focus (Gregorian focal plane)

3 Ray tracing analysis of the mapping from F_2 to F_1

The author expects that it is possible to calculate the focal points of the off-axis ellipsoidal subreflector analytically,² but this is not the approach used in this present work. Instead of analytical analysis, the mapping from the neighborhood of the second focus F_2 (i.e., the feed horn) to the neighborhood of the first focus F_1 has been determined by generating cones of rays at a grid of positions centered on the second focus and finding where these cones focus near the first focal point. Let us first consider the simple example shown in Figure 2 (note the 1:1 scale). Three cones of rays are shown, one originating at the second focal point in the center of the scene, one originating on-axis but 4 cm outside the focal point (on the left side) and the third cone originating 2 cm below F_2 . These three bundles of rays focus near the F_1 focal point as shown in Figure 3, with the first bundle forming a perfect focus and the other two focussing on caustic surfaces. The rectangular boxes in Figure 3 are $\pm 3\sigma$ error bars for the center points of the spherical wavefronts which best fit the path-lengths (wavefronts) of the converging cones of rays. The cone which originated 4 cm outside F_2 forms its focal point at 11.3 mm outside F_1 (it is the thin box on the right in Figure 3). This could be described as a longitudinal magnification of $3.54\times$, except that the focal point is also displaced 2.0 mm *laterally* above the axis because of the assymetry of the imaging system — we have only the abberations from one half of the ellipsoid, not balanced by abberations from the other half. The cone which originates 2 cm below F_1 in Figure 2 focusses at 5.4 mm above the axis and 8.0 mm inside F_1 (on the left) in Figure 3. Obviously, it is not reasonable to describe this situation as any kind of approximation of the simple longitudinal and lateral magnification which occurs in conventional on-axis Cassegrain and Gregorian systems. The full mapping from F_2 to F_1 can be obtained by tracing cones of rays for a grid of cases centered on F_2 . Such a grid of cones, with a spacing of 2 cm in X and Y , is shown in Figure 4, and the raytracing output is shown in Table 3.³ These results have been computed with the “ray” package [Wel98b], which was built by the author specifically for the GBT imaging problem, although the package has a generalized design.

²The case of an *on-axis* ellipsoid is definitely analytically tractable; see [Fan79].

³Only cases with displacements in X and Y have been traced, because the best static imaging performance will be obtained if the focal points are in the plane of symmetry. However, if we use motions of the subreflector to compensate for beam motions due to vibration [Wel96], we may want to translate images out of the plane of symmetry by rotating the subreflector about its Y_s axis. Therefore, the author expects that the grid of cases and the polynomial fitted to them will become 3-D in a future version of this software and report.

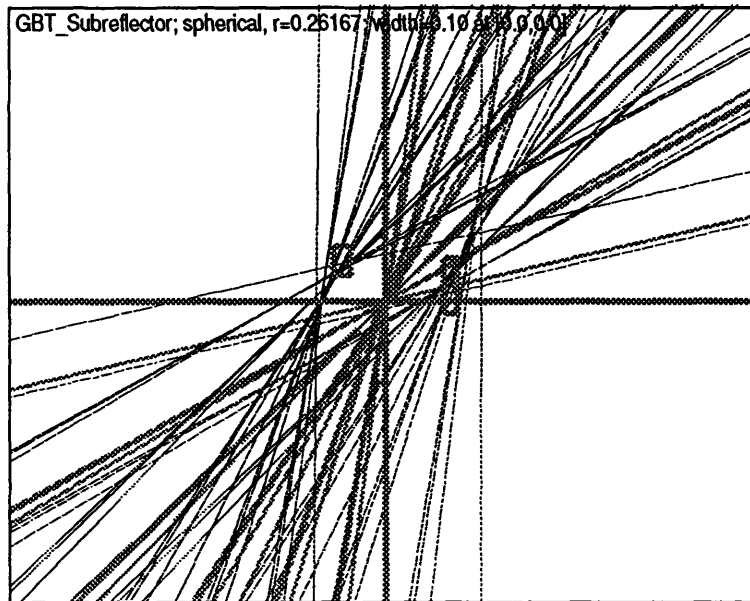


Figure 3: The three foci near the F_1 focus (Prime focal plane)

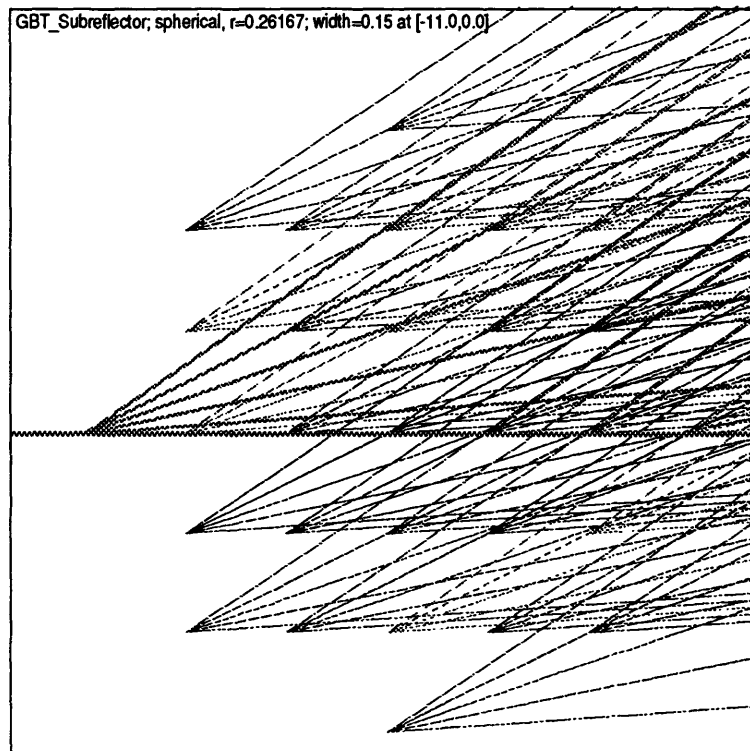


Figure 4: Multiple waves emitted near the Gregorian focal plane [srEllipsoidCase2b.ps]

```

# Ellipsoid Case#2: image grid of sources from F2 region onto F1 region
# D.Wells, NRAO-CV, 1995-08-11,08-31,09-17.
[GNU GPL copyright notice omitted]
# Command=<Digits 4 0.00001>
# Command=<System GBT_Subreflector>
#   unit is meters. origin at ellipsoid first focus (prime plane).
#   eps=0.528, e=5.5m, a=e/eps=10.4167m, b=sqrt(a^2-e^2)=8.8463m
#   r0=b^2/a=7.5126m, c=1/r0=0.133110, d=a-e=4.91667m
# Command=<rayAddSurface subreflector -0.133110 0.528 0 0 -1 4.91667 0 0 0 0|
#   | 0 cone 0 0 0 1 0 0 1>
#   tilt prime focus plane to 45.7d (prime focus box orientation):
# Command=<rayAddSurface prime_plane 0 0 0 0 1 0 0 0 0 0 0.798 cylinder 0 0 |
#   |0 1 0 0 1>
#   Generate spherical waves at grid around F2:
#   ray cone tilted by alpha=17.89878d=0.312393r
#   cone half-angle=14.993d=0.261677r
#   feed taper is -13db at 15d=0.26rad; sphere_wave_origins in 2_cm grid
# Command=<rayGenerator spherical -11 0 0 +0.902411 +0.312393 0 0.261677 0.0|
#   |2 3 6 2 0.261677 -13.0 2 13 bundle>
# Command=<rayTrace>
# Command=<rayGetFoci>
# Command=<rayPrtFoci>

      --< spherical, r=0.26167 >--
i      bundle_name  n      xc      yc      zc      lc      xs      ys      zs      ls
--      -----
1      -0.06 0 0 13  0.0129  0.0031 -0.0000  20.9047 0.0005 0.0019 0.0007 0.0018
2      -0.04 -0.04 0 13 -0.0030  0.0129 -0.0000  20.8905 0.0007 0.0006 0.0009 0.0008
3      -0.04 -0.02 0 13  0.0028  0.0075 -0.0000  20.8857 0.0004 0.0007 0.0004 0.0008
4      -0.04 0 0 13  0.0086  0.0021 -0.0000  20.8809 0.0003 0.0012 0.0005 0.0012
5      -0.04 0.02 0 13  0.0145 -0.0033 -0.0000  20.8763 0.0006 0.0019 0.0010 0.0018
6      -0.04 0.04 0 13  0.0205 -0.0086 -0.0000  20.8718 0.0010 0.0026 0.0016 0.0024
7      -0.02 -0.04 0 13 -0.0072  0.0119 -0.0000  20.8669 0.0007 0.0008 0.0010 0.0009
8      -0.02 -0.02 0 13 -0.0015  0.0065 -0.0000  20.8620 0.0003 0.0003 0.0004 0.0004
9      -0.02 0 0 13  0.0044  0.0010 -0.0000  20.8572 0.0002 0.0006 0.0002 0.0006
10     -0.02 0.02 0 13  0.0102 -0.0043 -0.0000  20.8525 0.0005 0.0013 0.0008 0.0012
11     -0.02 0.04 0 13  0.0162 -0.0097 -0.0000  20.8479 0.0009 0.0020 0.0014 0.0018
12     0 -0.06 0 13 -0.0171  0.0164  0.0000  20.8483 0.0012 0.0020 0.0017 0.0018
13     0 -0.04 0 13 -0.0114  0.0109 -0.0000  20.8432 0.0008 0.0013 0.0011 0.0012
14     0 -0.02 0 13 -0.0057  0.0055  0.0000  20.8383 0.0004 0.0007 0.0006 0.0006
15     0 0 0 13  0.0001  0.0000 -0.0000  20.8334 0.0000 0.0000 0.0000 0.0000
16     0 0.02 0 13  0.0060 -0.0054  0.0000  20.8287 0.0004 0.0007 0.0006 0.0006
17     0 0.04 0 13  0.0119 -0.0108 -0.0000  20.8241 0.0008 0.0014 0.0012 0.0013
18     0 0.06 0 13  0.0179 -0.0161  0.0000  20.8196 0.0012 0.0021 0.0018 0.0020
19     0.02 -0.04 0 13 -0.0157  0.0100 -0.0000  20.8196 0.0009 0.0019 0.0013 0.0016
20     0.02 -0.02 0 13 -0.0099  0.0045 -0.0000  20.8146 0.0005 0.0012 0.0008 0.0011
21     0.02 0 0 13 -0.0042 -0.0010 -0.0000  20.8097 0.0002 0.0006 0.0002 0.0006
22     0.02 0.02 0 13  0.0017 -0.0065 -0.0000  20.8049 0.0003 0.0003 0.0004 0.0004
23     0.02 0.04 0 13  0.0076 -0.0119 -0.0000  20.8002 0.0007 0.0009 0.0010 0.0009
24     0.04 -0.04 0 13 -0.0199  0.0090  0.0000  20.7960 0.0010 0.0024 0.0015 0.0021
25     0.04 -0.02 0 13 -0.0142  0.0035 -0.0000  20.7909 0.0006 0.0018 0.0010 0.0016
26     0.04 0 0 13 -0.0084 -0.0020  0.0000  20.7859 0.0003 0.0012 0.0005 0.0011
27     0.04 0.02 0 13 -0.0026 -0.0075 -0.0000  20.7811 0.0004 0.0007 0.0004 0.0008
28     0.04 0.04 0 13  0.0033 -0.0129 -0.0000  20.7764 0.0007 0.0006 0.0009 0.0008
29     0.06 0 0 13 -0.0127 -0.0030  0.0000  20.7622 0.0005 0.0018 0.0007 0.0017

# Command=<rayPltSystem>
# Command=<rayPltPS 12 12 0.15 -11.0 0.01 0. orthographic srEllipsoidCase2b.|
#   |ps>
# Command=<Quit>
    
```

Table 1: rayMain output for displacement grid

Table 2: Translation and tilt of the subreflector

Δx_2 (mm)	Δy_2 (mm)	Δx_1 (mm)	Δy_1 (mm)	σ_L (mm)	ΔS_{12} (mm)	$\Delta\phi$ (mr)	Δx_c (mm)	Δy_c (mm)
-60	0	12.9	3.1	1.8	72.9	0.28	-23.5	1.6
-40	-40	-3.0	12.9	0.8	37.1	4.79	-21.5	-13.5
-40	-20	2.8	7.5	0.8	42.8	2.49	-18.6	-6.2
-40	0	8.6	2.1	1.2	48.6	0.19	-15.7	1.1
-40	20	14.5	-3.3	1.8	54.5	-2.11	-12.8	8.3
-40	40	20.5	-8.6	2.4	60.6	-4.39	-9.8	15.7
-20	-40	-7.2	11.9	0.9	12.9	4.71	-13.6	-14.1
-20	-20	-1.5	6.5	0.4	18.5	2.41	-10.8	-6.8
-20	0	4.4	1.0	0.6	24.4	0.09	-7.8	0.5
-20	20	10.2	-4.3	1.2	30.2	-2.20	-4.9	7.8
-20	40	16.2	-9.7	1.8	36.3	-4.50	-1.9	15.2
0	-60	-17.1	16.4	1.8	-16.8	6.96	-8.6	-21.8
0	-40	-11.4	10.9	1.2	-11.3	4.63	-5.7	-14.6
0	-20	-5.7	5.5	0.6	-5.7	2.32	-2.9	-7.2
0	0	0.1	0.0	0.0	0.1	0.00	0.1	0.0
0	20	6.0	-5.4	0.6	6.0	-2.31	3.0	7.3
0	40	11.9	-10.8	1.3	12.0	-4.61	6.0	14.6
0	60	17.9	-16.1	2.0	18.2	-6.91	8.9	21.9
20	-40	-15.7	10.0	1.6	-35.6	4.56	2.2	-15.0
20	-20	-9.9	4.5	1.1	-29.9	2.23	5.0	-7.8
20	0	-4.2	-1.0	0.6	-24.2	-0.09	7.9	-0.5
20	20	1.7	-6.5	0.4	-18.3	-2.41	10.8	6.8
20	40	7.6	-11.9	0.9	-12.3	-4.72	13.8	14.1
40	-40	-19.9	9.0	2.1	-59.8	4.48	10.1	-15.5
40	-20	-14.2	3.5	1.6	-54.2	2.15	12.9	-8.2
40	0	-8.4	-2.0	1.1	-48.4	-0.18	15.8	-1.0
40	20	-2.6	-7.5	0.8	-42.6	-2.51	18.7	6.2
40	40	3.3	-12.9	0.8	-36.6	-4.83	21.6	13.5
60	0	-12.7	-3.0	1.7	-72.7	-0.27	23.6	-1.5

4 Translation of bisector ($\Delta x_c, \Delta y_c$) as a function of ΔS_{12} and $\Delta\phi$

The coordinates of the focal points themselves are not the most convenient variables to use in an algorithm for controlling the subreflector. Instead, it is better to use the change of separation of the desired foci ΔS_{12} and the tilt of the ellipsoid in the plane of symmetry $\Delta\phi$ as the independent variables, and the Δx_c and Δy_c translations of the center of the ellipsoid (described below) as the dependent variables. This representation of the ray tracing results can be computed as a least-squares fit to the raytracing output.

Various numerical results extracted from the raytracing output listing shown in Table 3 are tabulated in Table 2. The columns $\Delta x_2, \Delta y_2$ in Table 2 are the origins of the cones of rays near the ellipsoid focus F_2 ; they are plotted in Figure 5 (*cf* Figure 4). The corresponding displacements of the foci $\Delta x_1, \Delta y_1$ near F_1 , where these cones of rays focus, are shown in Figure 6. The reader can compare the three cases shown in Figures 2 and 3 with the corresponding points in Figures 5 and 6 in order to form an intuitive impression of the mapping function.

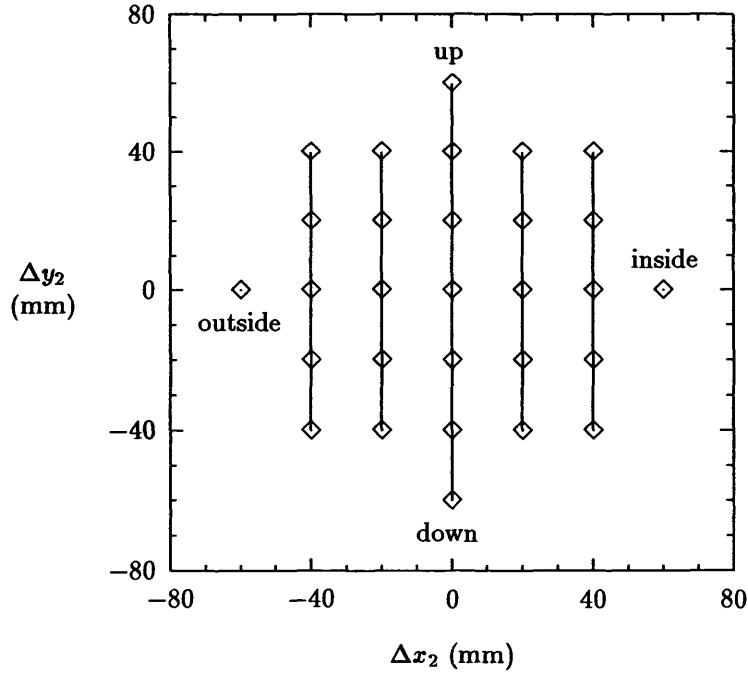


Figure 5: $\Delta x_2, \Delta y_2$ at F_2 from Table 2 (cf Figure 4)

The Euclidean separation between the pairs of foci in meters is

$$S_{12} = \sqrt{(11 + (\Delta x_1 - \Delta x_2))^2 + (\Delta y_1 - \Delta y_2)^2}; \quad (1)$$

the table shows the change of separation ΔS_{12} , which is given by

$$\Delta S_{12} = S_{12} - 11. \quad (2)$$

The tilt of the line connecting the points is given in the table by

$$\Delta \phi = \arctan \frac{\Delta y_1 - \Delta y_2}{11 + (\Delta x_1 - \Delta x_2)}. \quad (3)$$

The bisection point on the line connecting the two points (with length S_{12}) translates with respect to the center of the ellipsoid (bisection point between F_1 and F_2). The translation is given in the table by

$$\Delta x_c = \frac{\Delta x_1 + \Delta x_2}{2} \quad (4)$$

and

$$\Delta y_c = \frac{\Delta y_1 + \Delta y_2}{2}. \quad (5)$$

Variable σ_L in Table 2 (which is $1s$ in Table 3) is the RMS wavefront error of the converging rays at the foci near F_1 (see discussion in Section 6).

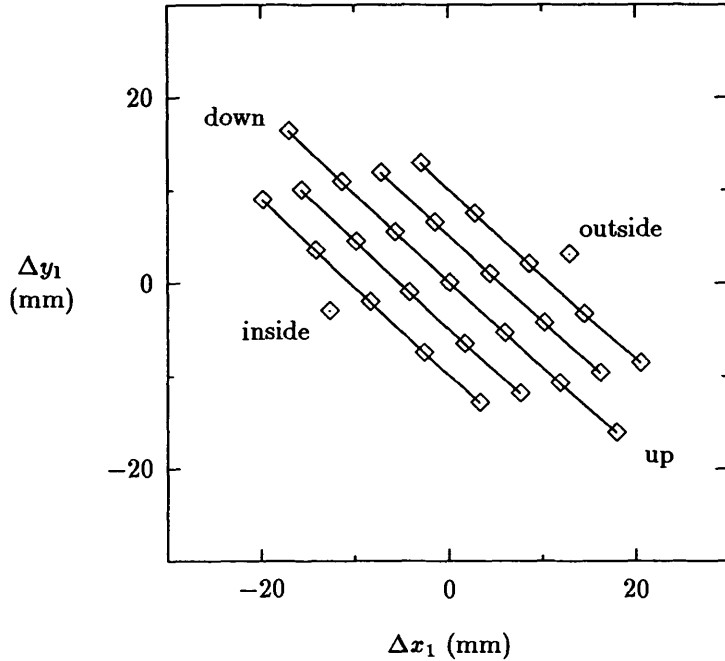


Figure 6: $\Delta x_1, \Delta y_1$ at F_1 from Table 2 (cf Figures 2 & 3)

5 Regression analysis: function `srEllipsoid()`

The least-squares regression has been done on four of the columns of Table 2 to fit Δx_c and Δy_c , the required translation of the *center* of the ellipsoid, as a function of ΔS_{12} and $\Delta\phi$, the excess length between the focal points and the extra tilt of the ellipsoid. Figure 7 shows the combinations of $\Delta\phi$ and ΔS_{12} which were traced and fitted. The regressions were done with Gaussfit [JFMM88], driven by an AWK [AKW88] program; the AWK program printed the results as C function `srEllipsoid()`, which is shown in Table 3. The fitted function is a simple polynomial in two independent variables; the two variables are scaled so that $(\pm 1, \pm 1)$ cover the range $(\pm 100, \pm 10)$ in $(\Delta S_{12}, \Delta\phi)$ [cf Figure 7]. The RMS of fit of the polynomials appears in comments in Table 3; it is 100μ or less. The fact that both of the polynomials are dominated by the same simple first-order terms is a strong hint that there is an analytic theory for the functions which are being fitted.

The dashed lines in Figure 8 are plotted from the output of function `srEllipsoid()` which incorporates the results of the regression, while the points are plotted from the raytrace results in Table 2, which are the inputs to the regression. This figure is a proof that the regression and code generation process have functioned correctly. The nearly straight, evenly spaced lines in this figure remind us again that the mapping is dominated by first-order terms.

The C function `srEllipsoid.c` shown in Table 3 is a key component of the GBT's Gregorian focus tracking algorithm [Wel98a].

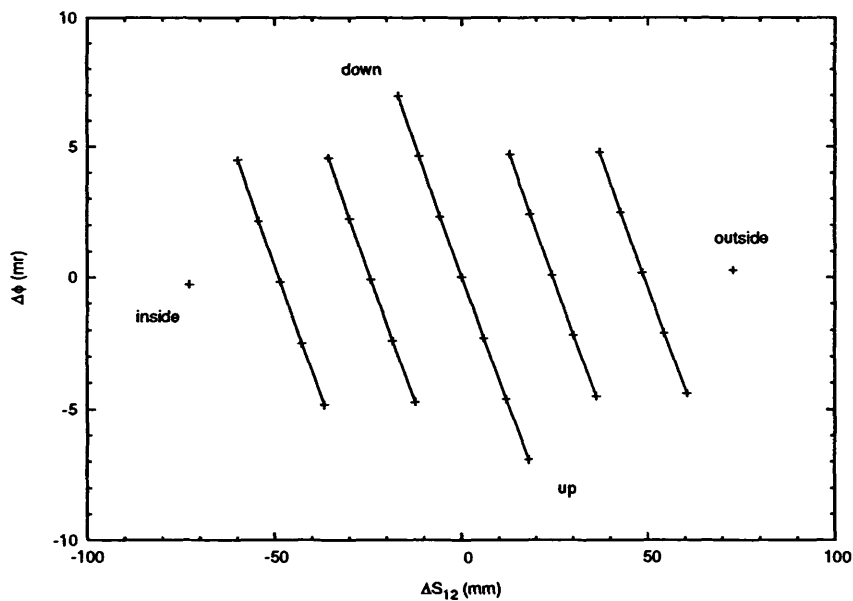


Figure 7: ΔS_{12} ($F_1 F_2 - 11m$), $\Delta\phi$ (axis-tilt) from Table 2

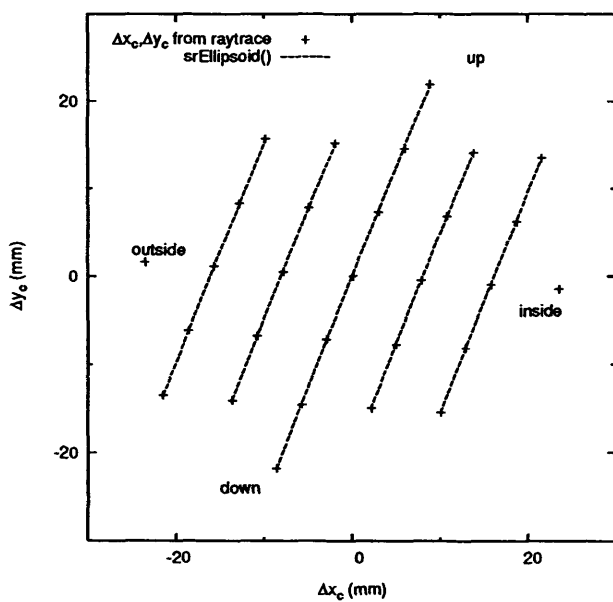


Figure 8: $\Delta x_c, \Delta y_c$ (center translation)

```

/* srEllipsoid.c -- center offset as function of separation and tilt */
[GNU GPL copyright notice omitted]
/* Computed 1998-03-16T21:37:05Z
   from least-squares fits to ray tracing data
   Don Wells <dwells@nrao.edu>, June-September 1995, May97 */
#include "srInclude.h"
void srEllipsoid (          /* void; dxyc[] is returned */
                  double s12, /* Separation=(F1F2-11m) (mm) */
                  double t,  /* Axis-tilt (mr) */
                  double dxyc[]) /* Center_offset (mm) */
{
    double *dxc, *dyc, s12p, tp;

    s12p = s12 / 100.0; /* fit valid over +/-10cm */
    tp = t / 10.0; /* fit valid over +/-10mr */

    dxc = &dxyc[0];
    dyc = &dxyc[1];
    dxyc[2] = 0.0;

    *dxc =
        (-31.6) * s12p
        + ( 0.2) * s12p*s12p
        + (-20.6) * tp
        + ( 0.8) * tp*tp
        + (-0.5) * s12p*tp;
    /* ( 0.1) sigma-of-fit for polynomial */

    *dyc =
        ( 3.3) * s12p
        + ( 0.2) * s12p*s12p
        + (-30.7) * tp
        + ( 0.1) * tp*tp
        + (-0.6) * s12p*tp;
    /* ( 0.0) sigma-of-fit for polynomial */
}

```

Table 3: Computed function srEllipsoid()

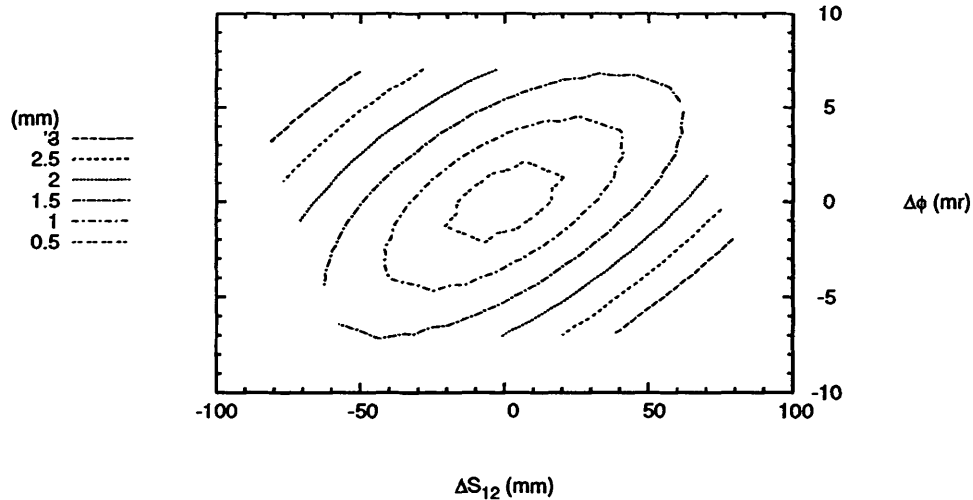


Figure 9: RMS phase error σ_L as function of ΔS_{12} and $\Delta\phi$

6 The ellipsoid phase error: function `srEllipsoidBestRms()`

Figure 9 shows contours of RMS phase error produced by the GBT ellipsoid operating with various values of ΔS_{12} and $\Delta\phi$. The contours are ellipses centered on the origin, where the RMS error is zero (the nominal optical prescription will be adjusted to focus perfectly at the rigging angle). Minimum phase error will be obtained along the major axes of these ellipses. I.e., minimum phase error will be obtained if the axis of the ellipsoidal subreflector is tilted by a few milliradians \pm *wrt* the line connecting the prime focal point and the Gregorian feed horn.

A simple algorithm searched the columns of the grid of numbers which produced the contour map in Figure 9, and produced a list of optimum $\Delta\phi$ values as a function of ΔS_{12} . This list was then fitted with a Chebyshev polynomial, using Gaussfit [JFMM88] driven by an AWK [AKW88] program. The fitted coefficients were printed as another C function `srEllipsoidBestRms()`, which is shown in Table 4. The RMS of fit was comparatively large, 0.4 mm; the author assumes that this was because the grid of cases which was searched was coarse.

The range of ΔS_{12} which occurs in the GBT focus tracking problem is -31 mm to +35 mm [Wel98a], which is comfortably covered by the grid of cases which have been computed in this work. In the focus tracking analysis [Wel98a], Zernike polynomials are fitted to the wavefronts traced from the Gregorian feed to the entrance pupil, as a function of elevation. The Zernike terms demonstrate that the extra tilt angle which is computed by `srEllipsoidBestRms()` compensates two of the third-order (Seidel) aberrations, spherical aberration and coma, and that the remaining phase errors are due to pure astigmatism. The author expects that it is possible to derive this fact analytically, probably by showing that the tilt is equivalent to a change of coordinates (variables) which cancels the third-order terms.

```

/* srEllipsoidBestRms.c -- dphi(ds12) for minimum subreflector RMS
/* Computed 1998-03-13T19:58:18Z
   from least-squares fits to ray tracing results
   Don Wells <dwells@nrao.edu>, Jan96,May97 */
[GNU GPL copyright notice omitted]
#include "srInclude.h"
double srEllipsoidBestRms (          /* returns extra_tilt=dphi   (mr) */
                           double ds12) /* delta_separation=(F1F2-11m) (mm) */
{
  double x = ds12 / 65.0; /* fit valid over +/- 65mm */
  double t0 = 1.0;
  double t1 = x;
  double t2 = 2.0*x*x      -1.0;
  double t3 = 4.0*x*x*x    -3.0*x;
  double t4 = 8.0*x*x*x*x  -8.0*x*x  +1.0;
  double t5 = 16.0*x*x*x*x*x -20.0*x*x*x +5.0*x;

  double dphi = ( -0.019) * t0
               + ( 5.404) * t1
               + ( -0.010) * t2
               + ( -0.327) * t3
               + ( 0.014) * t4
               + ( -0.535) * t5;
               /* ( 0.389) sigma-of-fit for Chebyshev polynomial */

  return(dphi);
}

```

Table 4: Computed function srEllipsoidBestRms()

A The On-Axis Case – “For the Record”

Many readers of this report are probably wondering whatever happened to the simple classical picture of the longitudinal and lateral magnifications of the on-axis ellipsoid. The author needed reassurance, too, and so Figures 10 and 11 have been computed. A grid of spherical wavefronts centered on F_2 was traced, just as before, but this time the ellipsoid was on-axis. The focal point analysis was done just as in Section 3, to produce Figure 11. The lines are nearly straight, evenly spaced, but now orthogonal to the axis of the ellipsoid. The comparison of the orthogonal lines in Figure 11 with the tilted lines in Figure 6 (p.8) again strongly hints that there is an analytical theory for these imaging properties.

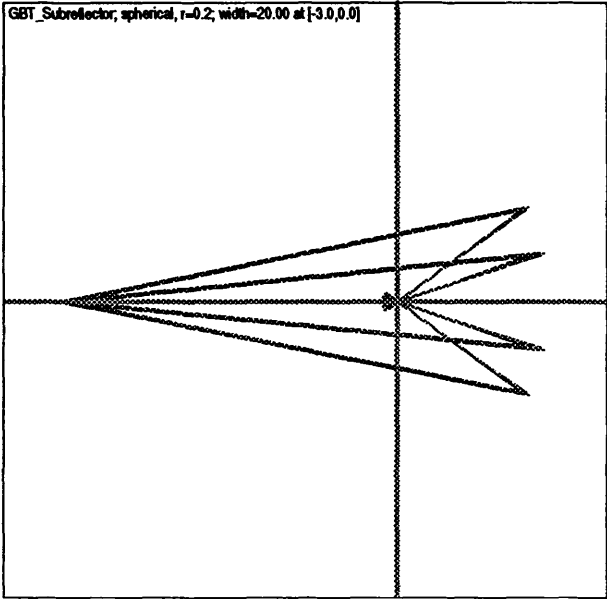


Figure 10: Overview of the On-Axis Case

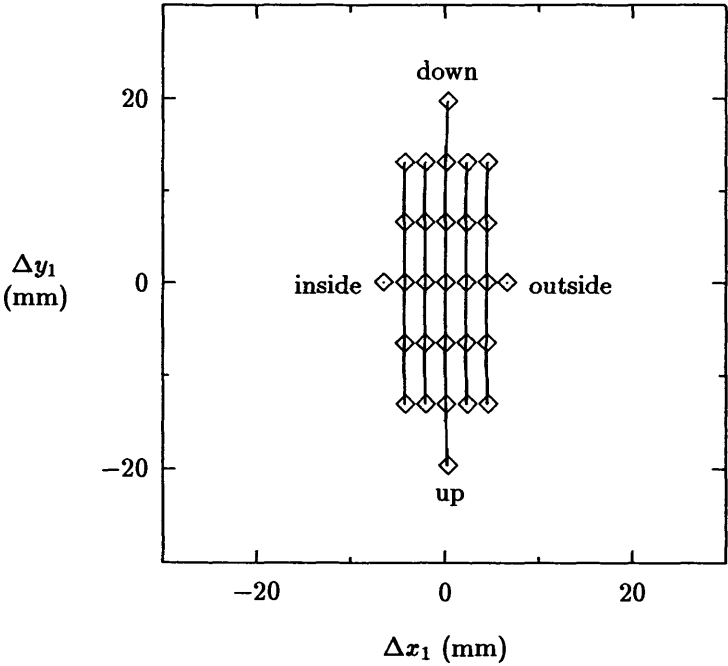


Figure 11: $\Delta x_1, \Delta y_1$ at F1 for the On-Axis Case

B Features expected to be added in future versions

- `srEllipsoid()`
 - Add third argument for yaw angle. This will be implemented by computing a grid of displacements out of plane of symmetry. This feature will support rotating subreflector about Y_s axis, which may be a feasible technique for tracking vibrations.
- `srEllipsoidBestRms()`
 - Add third argument for yaw angle? This may be needed if we decide to rotate the subreflector about Y_s axis for tracking vibrations, so that we get the best gain during the cyclic motion.
- This Memo
 - Generate a function in C to compute mean path length as a function of ΔS_{12} and $\Delta\phi$. This will support estimating phase corrections as a function of time to be applied to VLBI observations.

References

- [AKW88] Alfred V. Aho, Brian W. Kernighan, and Peter J. Weinberger. *The AWK programming language*. Addison-Wesley, New York, 1988. QA76.73.A95A35, ISBN 0-201-7981-X.
- [Fan78] Ronald L. Fante. A diffraction analysis of the elliptical reflector. In-House Report RADC-TR-78-42, Rome Air Development Center, Griffiss Air Force Base, New York, August 1978. “..for both the elliptic cylinder and the ellipsoid of revolution, the following calculations have been made: the magnitude of the fields near the foci, the size of the focal region, [and] the displacement of the focal spot as a function of the source displacement.. explicit results are presented for the fields as a function of the eccentricity of the ellipse and the angles subtended by the reflector edges”.
- [Fan79] Ronald L. Fante. An analysis of the elliptical reflector. *IEEE Trans. Antennas Propagat.*, AP-27(4):455–459, July 1979. “.this paper [is] a detailed study of the field distribution of the elliptic cylinder; the ellipsoid of revolution [was] studied [in [Fan78]].”.
- [JFMM88] William H. Jefferys, Michael J. Fitzpatrick, Barbara E. McArthur, and James E. McCartney. *User’s Manual — GaussFit: A system for least squares and robust estimation*. The University of Texas at Austin, 1.0-12/2/88 edition, December 1988. See <ftp://clyde.as.utexas.edu/pub/gaussfit/>.
- [NS96] R. Norrod and S. Srikanth. A summary of the GBT optics design. GBT Memo 155, National Radio Astronomy Observatory, March 1996.
- [Wel96] Don Wells. Approaches to the GBT vibration problem. GBT Memo 161, NRAO, December 1996. ‘The primary GBT vibration problem is that vibrations caused by wind turbulence are likely to be the major technical limitation for high frequency work throughout the life of the telescope’.
- [Wel98a] Don Wells. GBT Gregorian focus tracking in C. GBT Memo [tbd], NRAO, [in preparation] 1998. The GBT Gregorian subreflector, an off-axis portion of an ellipsoid, and the feedroom with the feedhorn move relative to the prime focal point of the main paraboloidal mirror. The subreflector must be maneuvered relative to the prime focal point and the feedhorn to maintain nearly stigmatic imaging (maximum gain, minimum sidelobes). An algorithm is described which computes the required actuator motions as a function of elevation, with *no* focus error, spherical aberration or coma, and with only 0.5 mm of residual astigmatism. The focus tracking algorithm is expressed in C.
- [Wel98b] Don Wells. The “ray” ray tracing package. GBT Memo 178, NRAO, March 1998. Abstract: “The ‘ray’ package and program rayMain trace sets of rays (representing wavefronts) through systems of rotationally-symmetric aspheric optical elements. The starting sets of rays can represent either plane or spherical wavefronts, with feedhorn tapering. The optical elements can be de-centered and/or tilted conic sections (planes, spheres, ellipsoids, paraboloids, hyperboloids) with additional superimposed radially-symmetric aspheric terms, and they can be mirrors as well as refracting surfaces. Both foci and nearly-plane wavefronts can be analyzed.” See ftp://fits.cv.nrao.edu/pub/gbt_dwells_ray.tar.gz (155 KB).